Modelling concentration heterogeneities in streets using the street-network model MUNICH

Thibaud Sarica[1], Alice Maison[1,2], Yelva Roustan[1], Matthias Ketzel[3], Steen Solvang Jensen[3], Youngseob Kim[1], Christophe Chaillou[4], and Karine Sartelet[1]

[1]CEREA, École des Ponts ParisTech, EDF R&D, IPSL, Marne-la-Vallée, 77455, France
[2]Université Paris-Saclay, INRAE, AgroParisTech, UMR EcoSys, 91120 Palaiseau, France
[3]Department of Environmental Science, Aarhus University, Roskilde, Denmark
[4]Aramco Fuel Research Center, Aramco Overseas Company, Rueil-Malmaison, 92500, France

Correspondence: Thibaud Sarica (thibaud.sarica@enpc.fr), Karine Sartelet (karine.sartelet@enpc.fr)

Abstract. Populations in urban areas are exposed to high local concentrations of pollutants, such as nitrogen dioxide and particulate matter, because of unfavorable dispersion conditions and the proximity to traffic. To simulate these concentrations over cities, models like the street-network model MUNICH (Model of Urban Network of Intersecting Canyons and Highways) rely on parameterizations to represent the air flow and the concentrations of pollutants in streets. In the current version MUNICH v2.0, concentrations are assumed to be homogeneous in each street segment. A new version of MUNICH where the street volume is discretized is developed to represent the street gradients and better estimate people exposure. Three vertical levels are defined in each street segment. A horizontal discretization is also introduced under specific conditions by considering two zones with a parameterization taken from the Operational Street Pollution Model (OSPM). Simulations are performed over two districts of Copenhagen, Denmark, and one district of Greater Paris, France. Results show an improvement of the comparison to observations with higher concentrations at the bottom of the street, closer to traffic, of pollutants emitted by traffic (NO_x, black carbon, organic matter). Finally, a sensitivity analysis to the influence of the street network highlights the importance to use the model MUNICH with a network rather than with a single street.

1 Introduction

Pollution is estimated to be responsible for approximately 9 million premature deaths in 2015 (Landrigan et al., 2018). This figure remains valid in 2019 despite an improvement of the types of pollution associated with extreme poverty (e.g., household air pollution and water pollution) (Fuller et al., 2022). This is partly due to an increase in the number of premature deaths attributable to ambient air pollution. The consequences of air pollution are particularly substantial in urban areas, where individuals are exposed to local high concentrations of air pollutants due to unfavorable dispersion conditions and proximity to traffic. As more than half of the world's population already lives in urban areas, rising to 68 % by 2050 (United Nations, 2019), it is crucial to estimate as accurately as possible the exposure of population to atmospheric pollutant concentrations in urban areas. For many years, various modelling approaches have been developed to contribute to the understanding of the phenomena

that drive the concentrations of pollutants in the atmosphere and to provide decision support tools (Collett and Oduyemi, 1997; Vardoulakis et al., 2003; El-Harbawi, 2013; Conti et al., 2017; Khan and Quamrul, 2021).

Regional-scale chemistry-transport models, such as Polair3D (Mallet et al., 2007; Sartelet et al., 2018), CHIMERE (Menut
25 et al., 2021; Falasca and Curci, 2018), CMAQ (Wong et al., 2012; de la Paz et al., 2015), represent the urban background concentrations by solving the chemistry-transport equation for spatial resolutions down to $1\,\mathrm{km}^2$. However, they can not represent street concentrations, which are often higher than background concentrations for pollutants such as NO_2 and particles (Lugon et al., 2020). To represent these concentrations, local-scale models are thus developed with different approaches of variable complexity and computational cost. Models based on computational fluid dynamics (CFD), such as code_saturne (Archambeau
30 et al., 2004; Gao et al., 2018), OpenFoam (Lin et al., 2022) and PALM (Wolf et al., 2020), are able to represent the dispersion of pollutants and the physicochemical processes taking place in urban districts and streets with a fine spatial resolution by solving the Navier-Stokes equations and mass conservation equations for pollutants. However, they suffer from high computational cost, as they use fine meshes to describe the morphology of buildings and streets. Other models use approaches that are less accurate than CFD but run faster. They are typically based on a Gaussian or an Eulerian approach (Vardoulakis et al., 2003;
35 Liang et al., 2023). Among these, can be mentioned ADMS-Urban (McHugh et al., 1997; Hood et al., 2021), SIRANE (Soulhac et al., 2011, 2023) and AERMOD (Cimorelli et al., 2004; Rood, 2014). They either consider each street independently of the others with exchanges between the street and the background concentrations above the street (Berkowicz, 2000a), or a street network with incoming/outcoming flows between streets at intersections (Soulhac et al., 2009; Kim et al., 2022). The Operational Street Pollution Model (OSPM) couples a Gaussian-plume model for traffic emissions and a box model for the
40 recirculation in the street (Berkowicz, 2000a). It is thus able to represent concentration heterogeneities in the street, but cannot include complex chemistry. The Model of Urban Network of Intersection Canyons and Highways (MUNICH) uses solely an Eulerian box-model approach (Lugon et al., 2020). As MUNICH is coupled with the SSH-aerosol model (Sartelet et al., 2020), the formation and aging of primary and secondary gas and particles in streets are represented. In the current version of MUNICH (v2.0) (Kim et al., 2022), concentrations are considered homogeneous in each street segment. However, as shown
45 by several on-site and modelling studies, the concentrations are very heterogeneous in streets with traffic emissions (Xie et al., 2003; Vardoulakis et al., 2011; Lateb et al., 2016; Sanchez et al., 2016; Amato et al., 2019; Lin et al., 2022). They are higher near the ground than at the top of the street, especially for primary pollutants.

A "heterogeneous" version of MUNICH is developed in this study aiming to represent the concentration heterogeneities in the street, while keeping the Eulerian approach of MUNICH to retain the ability to accurately model chemistry and aerosol
50 dynamics. The street volume is discretized vertically in three subvolumes. Traffic emissions are not instantaneously diluted in the whole street volume as in MUNICH v2.0, but only in the first subvolume, i.e. the one closest to the ground. To represent the street horizontal heterogeneities, a recirculation zone of the shape of a trapeze is defined, based on a parameterization of OSPM. It depends on the meteorological conditions and the street morphology, and it is applied under specific conditions in MUNICH that are described later.

55 A description of the differences between the homogeneous version of MUNICH (v2.0) and the new heterogeneous version is presented in Section 2. The applications to two street networks in Copenhagen, Denmark, with comparisons to observations

of NO_2 and CO, and to concentrations simulated by OSPM are discussed in Section 3. MUNICH is applied in Section 4 to the street network near Paris, France, used to validate MUNICH v2.0 (Kim et al., 2022), and the impacts of the heterogeneous version on concentrations of NO_2 and particles are studied. To estimate the impact of the modelling hypothesis on the transport

60 of pollutants between streets in the new version of MUNICH, a sensitivity analysis to the presence of a street network is performed in Section 5.

2 Model description

The homogeneous version of MUNICH (v2.0) and the new heterogeneous version (see Fig. 1) are briefly described in this section, focusing on the differences between the two versions. In the following, the homogeneous and heterogeneous versions

65 of MUNICH are referred to as MUNICH-homo and MUNICH-hete respectively. For a complete description of MUNICH, please refer to Kim et al. (2018, 2022) and Lugon et al. (2020, 2021a).

In order to solve the evolution equation of the street concentrations C_{str}, a first-order operator splitting between transport and chemistry is performed:

$$\frac{dC_{str}}{dt} = \frac{dC_{str}}{dt}\bigg|_{tr} + \frac{dC_{str}}{dt}\bigg|_{ch} \tag{1}$$

70 At each time step, the transport component is computed first. Chemical transformations are then applied to the resulting concentrations. As deposition and resuspension processes have minor effects compared to transport and chemistry (Lugon et al., 2021b; Kim et al., 2022), they are omitted in the rest of this study.

2.1 Homogeneous approach

Using a box-model approach, the concentrations are assumed to be homogeneous in the whole street volume and the effect of

75 the processes on the concentrations are represented by the equation:

$$\frac{dC_{str}}{dt}\bigg|_{tr} = \frac{1}{V}\left(Q_{em} + Q_{inflow} + Q_{outflow} + Q_{vert}\right) \tag{2}$$

with V the volume of the rectangular cuboid street, Q_{em} the traffic emission flux, Q_{inflow} the flux entering the street via the upwind intersection, $Q_{outflow}$ the flux leaving the street via the downwind intersection and Q_{vert} the vertical turbulent flux between the background and the street.

80 The street volume is defined as $V = HWL$, with H the mean building height in the street, W the mean street width and L its length. MUNICH considers that buildings on each side of the street are continuous, thus not representing inflow/outflow that could be induced by gaps in the buildings. The inflow term Q_{inflow} is obtained from the computation of the fluxes at the upwind intersection (Kim et al., 2018; Soulhac et al., 2009) (see Sec. 5 for a brief description). The outflow term $Q_{outflow}$ is expressed as :

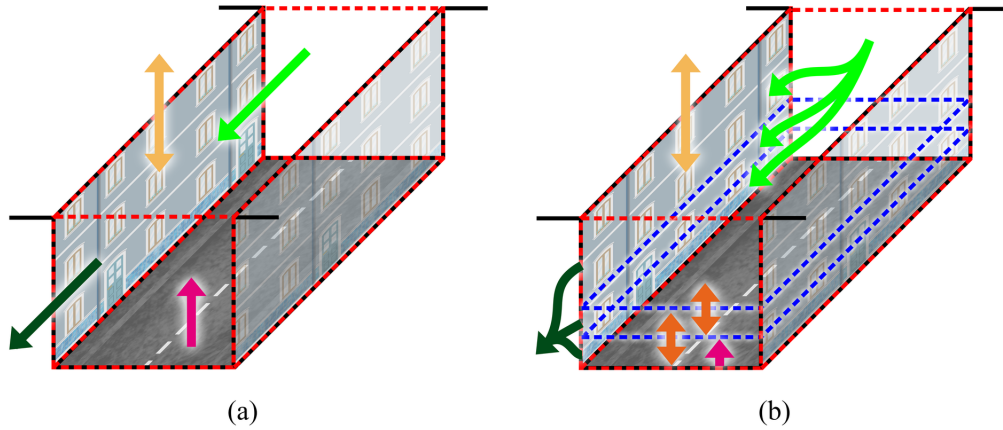85 $$Q_{outflow} = HWu_{str}C_{str} \tag{3}$$

Figure 1. Representation of the processes in the homogeneous version (a) and the heterogeneous version (b) of MUNICH. The red dotted lines represent the street volume. In (a), the street canopy is represented by a single volume, whereas in (b), it is divided into 3 subvolumes delimited by the blue dotted lines. The rose arrows represent the traffic emissions, the light green arrows the fluxes entering the street via the upwind intersection and the dark green arrows the fluxes leaving the street via the downwind intersection. The yellow arrows symbolize the vertical turbulent exchanges with the background and, in (b), the orange arrows the vertical exchanges among the subvolumes.

with u_{str} the mean horizontal wind speed in the street.

The vertical turbulent flux Q_{vert} between the street and the overlying atmosphere is:

$$Q_{\mathrm{vert}} = q_{\mathrm{vert}} W L \frac{(C_{\mathrm{str}} - C_{\mathrm{bkgd}})}{H} \tag{4}$$

with q_{vert} the vertical transfer coefficient and C_{bkgd} the background concentration.

90   The vertical transfer coefficient and the horizontal wind speed are the key parameters representing the dispersion of concentrations. As their formulation differs between the homogeneous and the heterogeneous versions of MUNICH, they are now detailed.

2.1.1 Vertical transfer coefficient for turbulent flux

Three parameterizations are implemented in MUNICH to determine the vertical transfer coefficient, q_{vert}, between the street
95 and the overlying atmosphere (Maison et al., 2022). However, currently only the parameterization adapted from Wang (2014) is designed to provide vertical profiles for both wind speed and mixing length within the street. We therefore limit our analysis to the latter.

In MUNICH-homo, the vertical transfer coefficient at the roof level is expressed as:

$$q_{\mathrm{vert}} = \sigma_{\mathrm{w}} l_{\mathrm{m}}(z=H) \quad \text{with} \quad l_{\mathrm{m}}(z) = \frac{\kappa z \, l_{\mathrm{c}}}{l_{\mathrm{c}} + \kappa z} \tag{5}$$

100 where σ_{w} is the standard deviation of the vertical wind velocity at roof level, l_{m} is the mixing length defined as a harmonic mean between two length scales (Coceal and Belcher, 2004) i) κz, with the Von Kármán constant ($\kappa = 0.42$) and ii) l_{c} a characteristic length of the street chosen equals to $0.5W$ (Maison et al., 2022).

2.1.2 Mean horizontal wind speed in the street

As for the calculation of the vertical transfer coefficient, three parameterizations are proposed in MUNICH to determine the

105 mean horizontal wind speed in the street (Maison et al., 2022). In the *Wang* parameterization, the mean horizontal wind speed in the street u_{str} is equal to:

$$u_{\mathrm{str}} = \frac{1}{H - z_{0s}} \int_{z_{0s}}^{H} u_Y(z)\,\mathrm{d}z = \frac{u_H |cos(\varphi)|}{(H - z_{0s})} \int_{z_{0s}}^{H} [J_1 I_0(g(z)) + J_2 K_0(g(z))]\,\mathrm{d}z \tag{6}$$

with $u_H |cos(\varphi)|$ the wind speed at roof level in the direction of the street and z_{0s} the wall and ground roughness length in the street (fixed to 0.01 m). I_0 and K_0 are the first and second kind modified Bessel function of order 0. J_1 and J_2 are integration

110 coefficients equal to:

$$J_1 = \frac{1}{I_0(g(H)) - I_0(g(z_{0s}))K_0(g(H))/K_0(g(z_{0s}))} \text{ and } J_2 = -\frac{J_1 I_0(g(z_{0s}))}{K_0(g(z_{0s}))} \tag{7}$$

The function $g(z)$ is calculated as:

$$g(z) = 2\sqrt{C_B a_r \frac{z}{l_{\mathrm{m}}(H)}} \tag{8}$$

with $a_r = H/W$ the aspect ratio of the street and C_B a coefficient dependent on the wind angle with the street and the aspect

115 ratio (Maison et al., 2022).

2.2 Heterogeneous approach

In MUNICH-hete, the street is divided into 3 vertical levels to limit the artificial dilution of the traffic emissions and the concentrations in the whole street volume (see Fig. 1(b) and Fig. 2). Levels are ordered from the ground to the top of the street. The first level (i=1) contains the traffic emissions. The thickness h_1 is taken as 2 m, which correspond to a zone where the

120 traffic producing turbulence mixes and dilutes traffic emissions (Solazzo et al., 2008). The second level (i=2) thickness h_2 is also of 2 m. It acts as a buffer zone between the first level where traffic emissions are and the third level where exchanges with the background take place. Starting at 4 m, the third level (i=3) goes to the roof level ($h_3 = (H - 4)$ m). The minimum street height considered in the model is set at $6\,m$. The three levels of the heterogeneous version are referred to as munich-hete-l1, munich-hete-l2 and munich-hete-l3 respectively. Each level i is thus associated to a specific volume, V_i, and the evolution

125 equations may be written as:

$$\frac{\mathrm{d}C_{\mathrm{str}}^i}{\mathrm{d}t}\bigg|_{\mathrm{tr}} = \frac{1}{V_i}\left(Q_{\mathrm{em}}^i + Q_{\mathrm{inflow}}^i + Q_{\mathrm{outflow}}^i + Q_{\mathrm{vert}}^{i,i+1} + Q_{\mathrm{vert}}^{i-1,i}\right) \tag{9}$$

with Q_{em}^i the traffic emission flux (only in the first level (i=1)), Q_{inflow}^i the flux entering the level via the upwind intersection, Q_{outflow}^i the flux leaving the level via the downwind intersection, $Q_{\mathrm{vert}}^{i,i+1}$ the vertical turbulent flux between the levels i and i+1 (for i=3, it exchanges with the background) and $Q_{\mathrm{vert}}^{i-1,i}$ the vertical turbulent flux between the levels i-1 and i (equals to zero if i=1).

In OSPM, the flow developing into a vortex in the street between buildings is represented by a recirculation zone. It occupies the whole street volume for narrow streets, and it has the shape of a trapeze for wider streets (Berkowicz et al., 1997; Berkowicz, 2000a; Ottosen et al., 2015). When the recirculation zone does not occupy the whole street volume, there is a ventilation zone (see Fig. 2) where concentrations of pollutants emitted by traffic are usually lower than in the recirculation zone. In MUNICH-homo, the recirculation zone is not explicited, whatever the street ratio H/W is. In MUNICH-hete, the volume of the recirculation zone is computed as in OSPM, as detailed in Appendix A. For now, concentrations in the ventilation zone are considered homogeneous and equal to the background concentrations, i.e. concentrations above the street. The ventilation zone is thus taken into account when it is not affected by traffic emissions. In practice, this means that the width of the trapeze base can only be equal to or larger than the width W of the street (see App. A). The width W_i of the level i can thus be inferior to the width W of the street, reducing the level volume (see Fig. 2). Appendix A presents the algorithm implemented in MUNICH-hete to consider the volume reduction of the ventilation zone. Further work is needed to differentiate the two zones for cases where the ventilation zone develops further into the street.

To quantify mass transfer through intersection, the fluxes are assumed to be vertically homogeneous and remain determined as proposed by Soulhac et al. (2009), as the shape of intersections may differ from one to another and turbulence is not quantified. The flux Q_{inflow} entering the street is assumed to be the same for each vertical level. The flux Q_{outflow} leaving a street is a surface-weighted average of the fluxes leaving each vertical level of the street:

$$Q_{\mathrm{outflow}} = \sum_{i=1}^{i=3} Q_{\mathrm{outflow}}^i = \sum_{i=1}^{i=3} S_i^v u_i C_{\mathrm{str}}^i \tag{10}$$

with S_i^v the vertical surface of the level i as presented in App. A and u_i the mean horizontal wind speed of the level i (see Sec. 2.2.2).

2.2.1 Vertical turbulent fluxes

To compute the vertical turbulent transfer $Q_{\mathrm{vert}}^{i,i+1}$ at the interface of the vertical levels i and i+1, Eq. 4 is modified to represent the vertical exchanges between the levels i and i+1:

$$Q_{\mathrm{vert}}^{i,i+1} = q_{\mathrm{vert}}^i W_i L \frac{(C_i - C_{i+1})}{\Delta z_i^{\mathrm{m}}} \tag{11}$$

with C_i and C_{i+1} the concentrations in the levels i and i+1 respectively, W_i the width of the level i that is inferior or equal to the width W of the street and Δz_i^{m} the difference in altitude between the middles of the levels i+1 and i, which are noted z_1^{m}, z_2^{m} and z_3^{m} (see Fig. 2). For i=3, i.e. the highest level, z_{i+1}^{m} is taken as the symmetrical of z_3^{m} to the roof level, and noted $z_{\mathrm{bkgd}}^{\mathrm{m}}$. It gives an approximation of the volume that effectively exchanges with the third level.
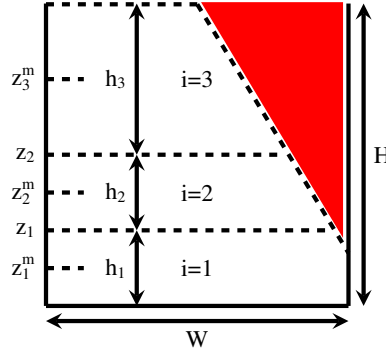
Figure 2. Schematic of the discretization in MUNICH-hete. The red triangle represent the ventilation zone that is present under specific conditions, and the white trapeze represents the recirculation zone. z_i^m is the middle height of level i.

Among the three parameterizations implemented in MUNICH to determine the vertical transfer coefficient q_{vert}, only the *Wang* parameterization is adapted to the discretization. It is thanks to its explicit vertical dependency and validity for a wide

160 range of street-canyon and wind characteristics (Maison et al., 2022). To compute the vertical turbulent transfer $Q_{\mathrm{vert}}^{i,i+1}$, the vertical transfer coefficient is taken at the height of the interface between the two vertical levels considered, and Eq. 5 is now written as:

$$q_{\mathrm{vert}}^i = \sigma_{\mathrm{w}} \kappa z_i \frac{l_{\mathrm{c}}}{l_{\mathrm{c}} + \kappa z_i} \tag{12}$$

with z_i the height of the interface between levels i and i+1.

165 By combining Eq. 11 and Eq. 12, the vertical turbulent transfer $Q_{i,i+1}$ can be written for each level as:

$$Q_{\mathrm{vert}}^{1,2} = \sigma_{\mathrm{w}} \kappa z_1 \frac{l_{\mathrm{c}}}{l_{\mathrm{c}} + \kappa z_1} W_i L \frac{C_1 - C_2}{z_2^m - z_1^m} \tag{13}$$

$$Q_{\mathrm{vert}}^{2,3} = \sigma_{\mathrm{w}} \kappa z_2 \frac{l_{\mathrm{c}}}{l_{\mathrm{c}} + \kappa z_2} W_i L \frac{C_2 - C_3}{z_3^m - z_2^m} \tag{14}$$

$$Q_{\mathrm{vert}}^{3,\mathrm{bkgd}} = \sigma_{\mathrm{w}} \kappa H \frac{l_{\mathrm{c}}}{l_{\mathrm{c}} + \kappa H} W_i L \frac{C_3 - C_{\mathrm{bkgd}}}{z_{\mathrm{bkgd}}^{\mathrm{m}} - z_3^m} \tag{15}$$

with C_1, C_2, C_3 and C_{bkgd} the concentrations of the three levels and the background respectively.

170 ### 2.2.2 Mean horizontal wind speed in the street

As for the vertical turbulent flux, only the *Wang* parameterization among the three parameterizations available in MUNICH can be used to compute the mean horizontal wind speeds in the street. It is thanks to its explicit vertical dependency and the no-slip condition at the ground that is always satisfied (Maison et al., 2022). Therefore, the mean horizontal wind speed can be computed at each level in the street, by modifying Eq. 6 to integrate vertically between the level heights:

$$u_1 = \frac{1}{z_1 - z_{0s}} \int_{z_{0s}}^{z_1} u_Y(z)\,\mathrm{d}z \tag{16}$$

$$u_2 = \frac{1}{z_2 - z_1} \int_{z_1}^{z_2} u_Y(z)\,\mathrm{d}z \tag{17}$$

$$u_3 = \frac{1}{H - z_2} \int_{z_2}^{H} u_Y(z)\,\mathrm{d}z. \tag{18}$$

with z_1 and z_2 the limits of the first two levels as presented in Fig. 2.

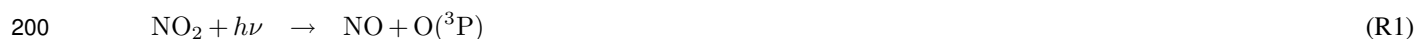## 3 Application to street networks in Copenhagen with comparison to OSPM

This section presents two applications of MUNICH-hete to assess its capabilities compared to MUNICH-homo and OSPM. Simulations are performed over the year 2019 for two street networks in Copenhagen, Denmark. The first street network is centered around the H. C. Andersens Boulevard and the second around the Jagtvej street. They are named HCAB and JGTV respectively in the following. They have been selected as observational data of CO, NO_2, NO_x and O_3 are available for the HCAB and, NO_2 and NO_x for JGTV over the whole year. OSPM simulations were also performed to compare model performances. As OSPM does not represent air fluxes at intersections, OSPM simulations are performed only for the streets where there are observations. Thanks to its coupled approach between a Gaussian plume model and a box model, OSPM is able to calculate concentrations on the two sides of the street (Berkowicz et al., 1997; Berkowicz, 2000a; Ottosen et al., 2015). Two receptors are used to compare with the observed concentrations on each side of the street: OSPM-R1 and OSPM-R2. The height of the receptors is taken as 2 m to correspond roughly to the height at which observations were performed. They are compared to the concentrations simulated at the first two levels of MUNICH-hete, which are representative of the concentrations at 1 m and 3 m.

MUNICH and OSPM use the same input data to estimate the street concentrations. The meteorological parameters originate from WRF simulations (Skamarock et al., 2008) and the background concentrations are simulated using the Urban Background Model (UBM) (Berkowicz, 2000b). Traffic emissions are generated using the OML-Highway model (Olesen et al., 2015) allowing for precise information for each street segment.

OSPM represents NO_2 and O_3 chemical transformations using a system of 2 reactions (Berkowicz et al., 1997; Berkowicz, 2000a). The first one describes the production of NO_2 due to reaction of NO with O_3, and the second one the photodissociation of NO_2 leading to reproduction of NO and O_3. For a fair comparison, MUNICH is configured to run with a simple chemistry

Geoscientific
Model Development
Discussions

scheme, the Leighton photostationary state for O_3 (Leighton, 1961; Kim et al., 2018):

$$NO_2 + h\nu \quad \rightarrow \quad NO + O(^3P) \tag{R1}$$

$$O(^3P) + O_2 + M \quad \rightarrow \quad O_3 + M \tag{R2}$$

$$NO + O_3 \quad \rightarrow \quad NO_2 + O_2 \tag{R3}$$

3.1 H. C. Andersens Boulevard

H. C. Andersens Boulevard is a wide, densely-trafficked boulevard, with an aspect ratio $a_r = H/W$ of about 0.2. It is open on one side with trees instead of buildings. This configuration can be represented in OSPM. However, in MUNICH, a mean building height is defined for each street. Here, it is estimated by averaging the building and the tree heights. The simulated street network is composed of 86 street segments centered around the street where the observation station is located (see brown cross on Fig. 4). Figure 3 presents the monthly-averaged concentrations of CO and NO_2 from the OSPM and MUNICH simulations compared to observations. Appendix C contains monthly-averaged concentrations of NO_x and O_3, and statistical indicators of the comparison for all four pollutants.

OSPM-R1 is the receptor that is close to the measurement station, thus better suited to be compared to observations. Differences in concentrations between OSPM-R1 and OSPM-R2 highlight the importance to take into account horizontal heterogeneities in the street. Observations lies between the concentrations simulated at the two receptors, except for CO for which OSPM slightly underestimates concentrations in the first half of the year. This underestimation could be linked to underestimation of sources other than traffic, e.g. biomass burning, at the regional scale. Overall, the concentrations are well estimated with OSPM with errors between 26% and 33% for CO, and between 34% and 46% for NO_2.

For CO, NO_2 and NOx, which are emitted by traffic in the bottom of the street, the concentrations are higher in the first level MUNICH-hete-l1 near the bottom and lower in the third level near the roof level. For O_3, the opposite behavior is observed as it is mainly imported by the atmosphere above the street, and it is titrated by NO near the ground. The first two levels munich-hete-l1 and munich-hete-l2 have higher concentrations of CO, NO_2 and NO_x than munich-homo, thus improving the comparison to observations and OSPM concentrations. For CO, the error is improved from 36% in MUNICH-homo to 28% in MUNICH-hete-l1, and for NO_2, it is improved from 48% in MUNICH-homo to 35% in MUNICH-hete-l1. Although the concentrations of NO_2 and CO are underestimated in MUNICH-homo compared to observations, they are well modelled in the first level MUNICH-hete-l1 with low errors and biases (see Appendix C). For CO, the concentrations simulated in the first level MUNICH-hete-l1 lies between the two OSPM receptors for most of the year. This is the case for NO_2 as well, except between April and August, when NO_2 concentrations are underestimated in MUNICH-hete. The formation of NO_2 in the lower levels (see Reaction R3) could be limited with the current model setup, because volatile organic compounds are not taken into account in the Danish cases. However, they may participate in O_3 and NO_2 formation through HO_2 and RO_2 radicals (Atkinson, 2000; Kwak and Baik, 2012; Zhong et al., 2017; Dai et al., 2021). Furthermore, the vertical discretization is coarse, limiting O_3 transport deep into the street.
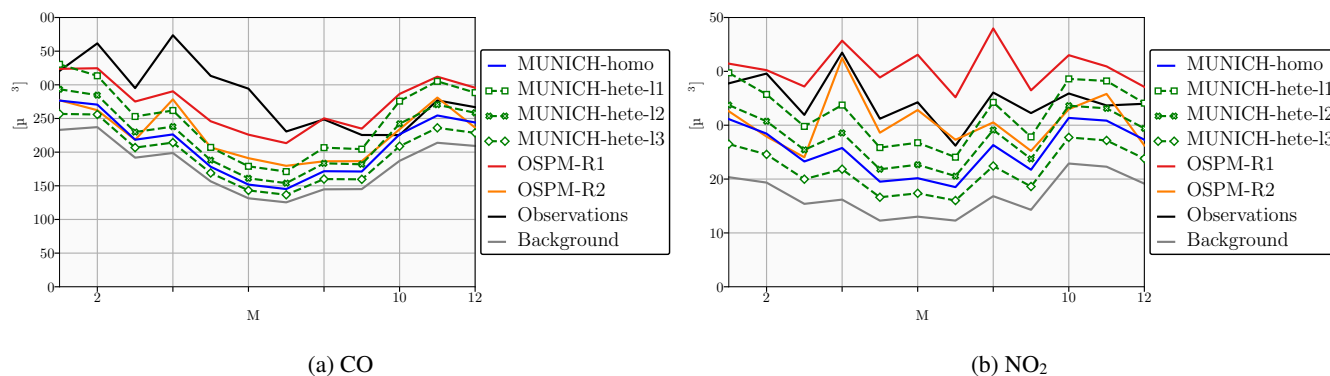
(a) CO

(b) NO$_2$

Figure 3. Monthly-average concentrations (in µg m^{-3}) of CO (a) and NO$_2$ (b) at HCAB monitoring station. The solid blue line represents the homogeneous version of MUNICH. The three green dashed lines represents the three levels of the heterogeneous version of MUNICH, the lowest level (l1) with square markers, the intermediate level (l2) with cross markers and the top level (l3) with diamond markers. The solid red line represents the OSPM receptor that is close to the measurement station and the solid orange line the second OSPM receptor located on the other side of the street. The observations are in solid black and the background concentrations in solid grey.

Over the whole street network, as presented in Fig. 4, the differences between the concentrations simulated in the first vertical level of MUNICH-hete compared those simulated in MUNICH-homo vary. For wide streets and avenue with dense traffic, the concentrations are higher in MUNICH-hete-l1 than in MUNICH-homo, with an increase by up to 23 % for CO and 30 % for NO$_2$. This increase is lower in more narrow and less frequented streets. Although the concentrations in MUNICH-hete-l1 are always higher than those in MUNICH-homo for CO, for NO$_2$, in narrow streets, the concentrations are lower in MUNICH-hete-l1. These lower NO$_2$ concentrations are probably related to the limited transport of O$_3$ from the background to the bottom of the street, limiting the titration of NO.
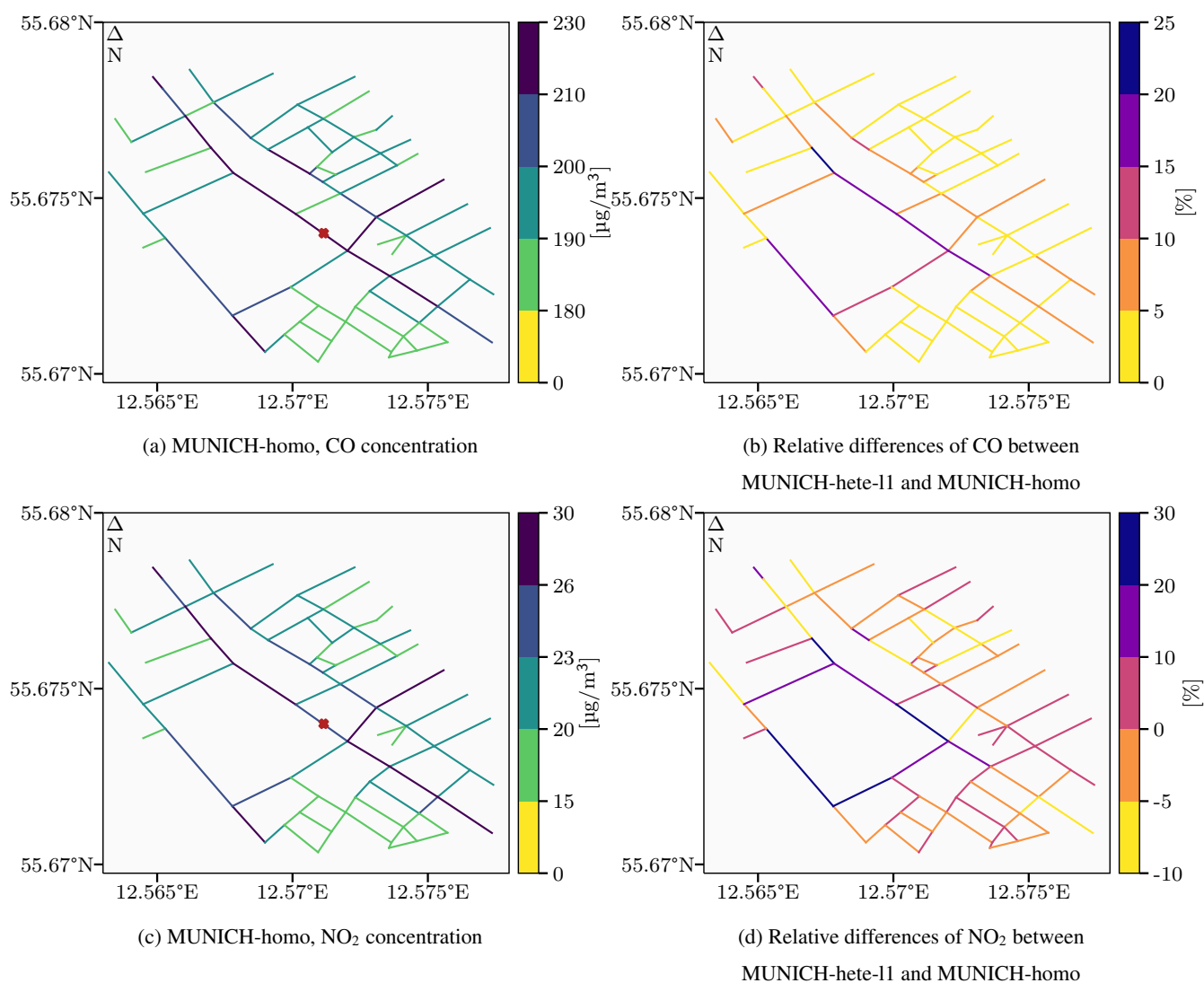
(a) MUNICH-homo, CO concentration

(b) Relative differences of CO between
MUNICH-hete-l1 and MUNICH-homo

(c) MUNICH-homo, NO$_2$ concentration

(d) Relative differences of NO$_2$ between
MUNICH-hete-l1 and MUNICH-homo

Figure 4. CO and NO$_2$ time-averaged concentrations (in µg m^{-3}) for MUNICH-homo on the upper and lower left panels respectively for the HCAB street network. Relative differences (in %) between the first level of MUNICH-hete and MUNICH-homo for CO and NO$_2$ on the upper and lower right panels respectively for the HCAB street network. A positive relative difference indicates higher concentrations for MUNICH-hete. The brown cross on panels (a) and (c) represents the position of the measurement station.

Geoscientific
Model Development
Discussions

3.2 Jagtvej

Jagtvej is a conventional street canyon with an aspect ratio of about 0.8. The simulated street network is composed of 265 street

240 segments centered around the street where the observation station is located (see brown cross on Fig. 6). The monthly-averaged

concentrations of CO and NO_2 from the OSPM and MUNICH simulations compared to observations are presented in Fig. 5.

Appendix D contains monthly-averaged concentrations of NO_x and O_3, and statistical indicators of the comparison for NO_2

and NO_x.

OSPM-R2 is the receptor that is close to the measurement station, thus better suited to be compared to observations. The

245 differences between the concentration of the two OSPM receptors are lower in JGTV than in HCAB (see Fig. 3). JGTV is

narrower with higher buildings on both sides, thus limiting the ventilation zone and the penetration in the street of background

concentrations that would reduce the concentrations at the downwind receptor. OSPM tends to slightly overestimate NO_2 and

NO_x concentrations (with errors between 41% and 53% and between 42% and 63% respectively).

Concentrations from the homogeneous version of MUNICH are close to OSPM concentrations for CO. They are lower

250 than OSPM concentrations for NO_2, but they compare well to observations with a bias of -3%, and an error of 46%. These

lower NO_2 concentrations are linked to lower NO_x concentrations (with a bias of -19% compared to observations and an error

of 53%). As for HCAB, the MUNICH-hete concentrations decrease from the bottom to the top of the street. For CO and

NO_x, only the first level have concentrations higher than MUNICH-homo while for NO_2, all three levels have concentrations

lower than MUNICH-homo. O_3 concentrations are also higher for the three levels (see Fig. D1). The NO_x concentrations of

255 MUNICH-hete-l1 compare slightly better to observations than MUNICH-homo, while MUNICH-homo is slightly better for

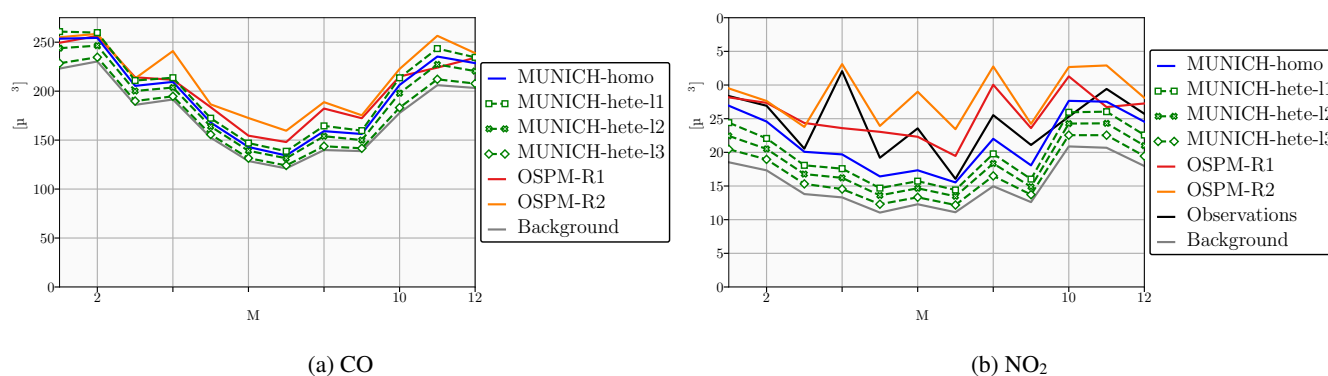NO_2. However, the statistics of the two models are quite close (Appendix D).

(a) CO

(b) NO_2

Figure 5. Monthly-average concentrations (in $\mu g\,m^{-3}$) of CO (a) and NO_2 (b) at JGTV monitoring station. The solid blue line represents the homogeneous version of MUNICH. The three green dashed lines represents the three levels of the heterogeneous version of MUNICH, the lowest level (l1) with square markers, the intermediate level (l2) with cross markers and the top level (l3) with diamond markers. The solid orange line represents the OSPM receptor that is close to the measurement station and the solid red line the second OSPM receptor located on the other side of the street. The observations (only available for NO_2) are in solid black and the background concentrations in solid grey

Conclusions are similar for the whole street network (see Fig. 6). The CO concentrations are slightly higher in the first level of MUNICH-hete than in MUNICH-homo. However, NO_2 concentrations at the bottom of the street in the first level of MUNICH-hete tend to be lower than in MUNICH-homo. In some specific street segments of the network, the differences of concentrations for both CO and NO_2 are higher in MUNICH-hete-l1 than in MUNICH-homo. This is due to a mix of different traffic emissions and street morphologies which favor the transport of pollutants.
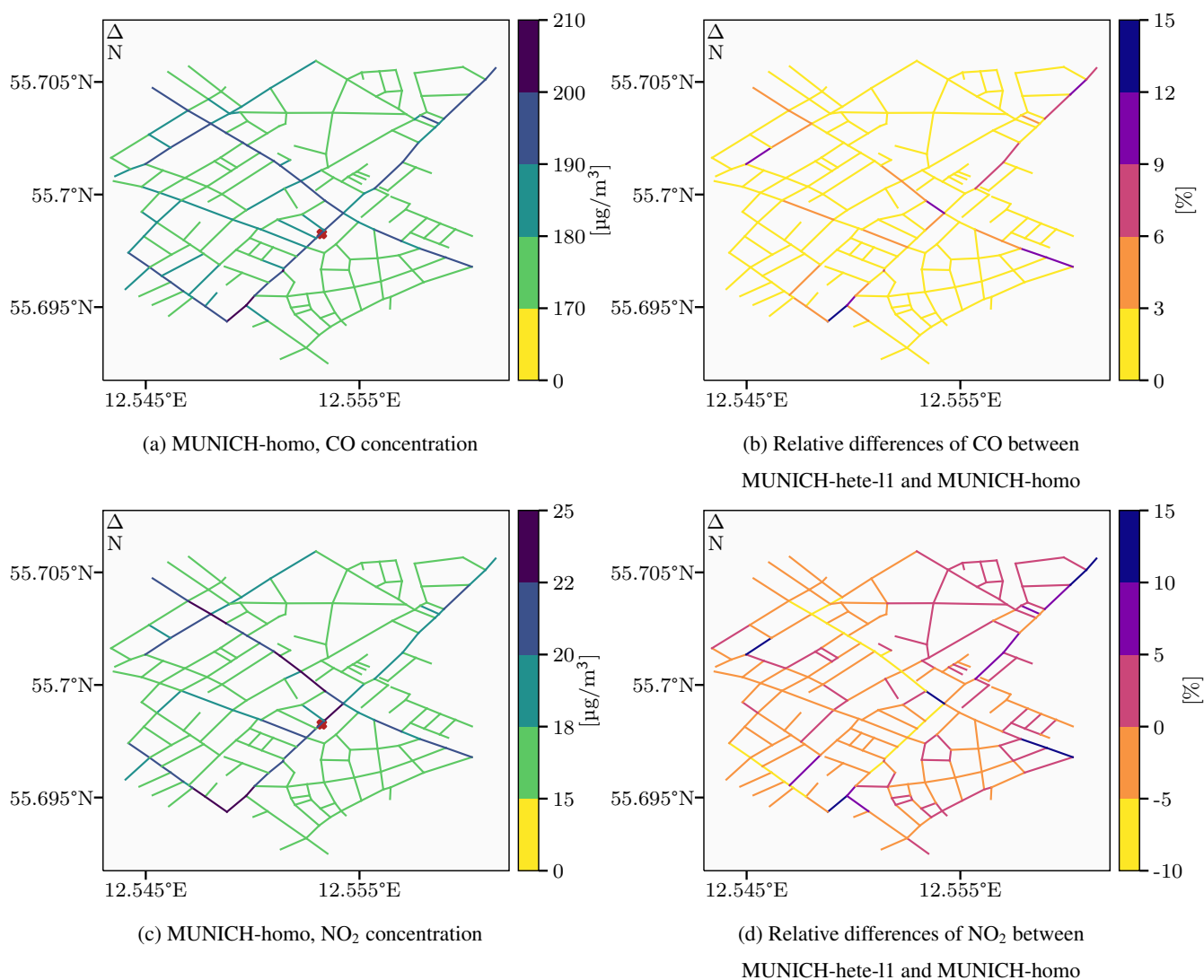

(a) MUNICH-homo, CO concentration

(b) Relative differences of CO between
MUNICH-hete-l1 and MUNICH-homo

(c) MUNICH-homo, NO_2 concentration

(d) Relative differences of NO_2 between
MUNICH-hete-l1 and MUNICH-homo

Figure 6. CO and NO_2 time-averaged concentrations (in µg m⁻³) for MUNICH-homo in the upper and lower left panels respectively for the JGTV street network. Relative differences (in %) between the first level of MUNICH-hete and MUNICH-homo for CO and NO_2 in the upper and lower right panels respectively for JGTV. A positive relative difference indicates higher concentrations for MUNICH-hete. The brown cross on panels (a) and (c) represents the position of the measurement station.

4 Application to a street network in Greater Paris

The impacts of the discretization on gas and particle concentrations is evaluated over the street network near Paris, France, which was used to validate MUNICH v2.0 (Kim et al., 2022) and in several sensitivity studies (Lugon et al., 2021b; Sarica

265 et al., 2022). The street network represents a district of Le Perreux-sur-Marne, a suburb 13 km east of Paris, France. It is composed of 577 street segments (see Fig. 8). Simulations are performed from 22 March to 15 June 2014 with input data (emissions, meteorological parameters and background concentrations) from the reference simulation SCN0 of Sarica et al. (2022). Observational data are available for the whole simulation period for NO_2, NO_x, $PM_{2.5}$, PM_{10} and black carbon (BC) at a segment of Boulevard d'Alsace Lorraine (see brown cross on Fig. 8). They were performed at a height of about 2 m and they

270 are thus to be compared to the concentrations of the first two levels (i=1 and i=2) of MUNICH-hete.

The average daily profiles of NO_x and PM_{10} concentrations are shown in Fig. 7, and for NO, NO_2 and the statistical indicators in Appendix E1. As in the Danish streets, for pollutants emitted by traffic, the concentrations are higher in MUNICH-hete at the bottom of the street decreasing to the roof level. The concentrations of PM_{10}, NO_2, NO_x and BC are higher on average by 12 %, 21 %, 40 % and 30 % respectively in MUNICH-hete-l1 than in MUNICH-homo. The lower concentration difference for PM_{10}

275 than for the other compounds reflects that non-traffic sources are more important for PM_{10}, and inversely they are small for BC. Despite the higher concentrations in MUNICH-hete-l1, BC concentrations remain strongly underestimated compared to observations, in agreement with the CFD simulations of Lin et al. (2022). For PM_{10}, NO_2 and NO_x, the concentrations compare well to observations, e.g. the error is 33% for NO_2 and 37% for PM_{10}, with slightly better statistics using MUNICH-hete-l1 than MUNICH-homo. For all pollutants, the concentrations of the intermediate level (i=2) are very close to the concentrations

280 of MUNICH-homo. This is due to a mixture of different parameters such as street morphology and dispersion conditions over the simulated period.
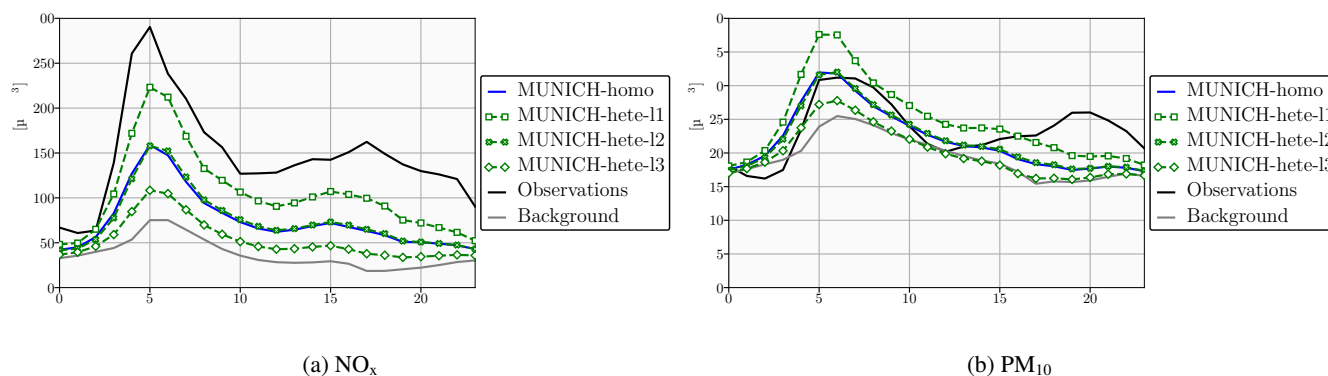

(a) NO_x (b) PM_{10}

Figure 7. Average daily profile of the concentrations of NO_x (a) and PM_{10} (b) over the simulation period at the Boulevard d'Alsace Lorraine monitoring station. The solid blue line represents the homogeneous version of MUNICH. The three green dashed lines represents the three levels of the heterogeneous version of MUNICH, the lowest level (l1) with square markers, the intermediate level (l2) with cross markers and the top level (l3) with diamond markers. The observations are in solid black and the background concentrations in solid grey

In streets, both BC and organic matter (OM) exhibit higher concentrations than in the background (Lugon et al., 2021a). OM consists of primary and secondary aerosols that are formed from the oxidation of volatile organic compounds and/or the condensation of semi-volatile organic compounds. Concentrations of both BC and OM simulated in MUNICH-homo and in the first level of MUNICH-hete are compared in Fig 8 (see Appendix Fig. E2 for NO_2 and PM_{10}). The concentrations simulated in MUNICH-hete-l1 are always higher than in MUNICH-homo. In most streets of the network that are narrow and with limited traffic, the increase in concentrations is limited. It is more important for more open and frequented streets, such as the Boulevard d'Alsace Lorraine.

BC being a primary inert pollutant emitted by traffic, its concentrations are strongly influenced by the discretization as emissions are no longer artificially diluted in the whole street volume. They are now constraint at the bottom of the street inducing an average increase of 30 % compared to the homogeneous version. For OM and PM_{10}, the increase is lower (16 % and 12 % respectively), because of the stronger influence of non-traffic sources.
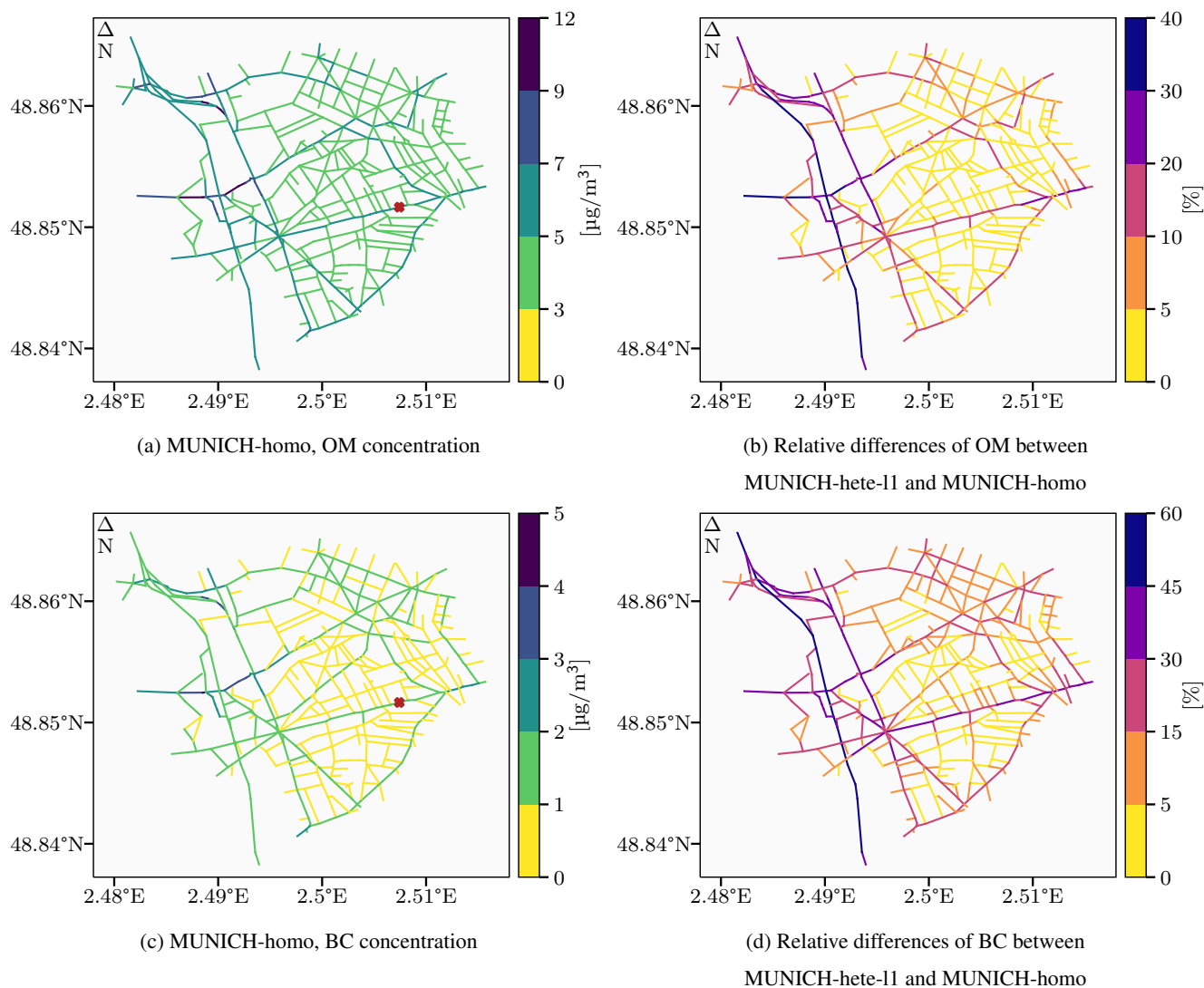
(a) MUNICH-homo, OM concentration

(b) Relative differences of OM between
MUNICH-hete-l1 and MUNICH-homo

(c) MUNICH-homo, BC concentration

(d) Relative differences of BC between
MUNICH-hete-l1 and MUNICH-homo

Figure 8. OM and BC time-averaged concentrations (in µg m^{-3}) for MUNICH-homo in the upper and lower left panels respectively for the district of Le Perreux-sur-Marne. Relative differences (in %) between the first level of MUNICH-hete and MUNICH-homo for OM and BC in the upper and lower right panels respectively for the district of Le Perreux-sur-Marne. A positive relative difference indicates higher concentrations for MUNICH-hete. The brown cross on panels (a) and (c) represents the position of the measurement station.

5 Sensitivity analysis

In this section, the sensitivity of the heterogeneous version of MUNICH to the presence of a street network, which influences
295 the concentrations entering the street via the upwind intersection, is estimated.

The computation of inflow and outflow fluxes at intersections is performed by estimating the balance of fluxes entering and
leaving the intersection from the different street segments attached to it. If this balance is not perfect, there are exchanges with
the atmosphere above the intersection. When the total flux entering the intersection is higher than the one leaving it, the flow
overload is directed to the atmosphere. When the total flux leaving the intersection is higher, a flux from the atmosphere to the
300 intersection is considered. Further explanation is available in Kim et al. (2018, 2022).

Without a street network around the street segment of interest, the pollutant mass fluxes entering the street are determined
from the background concentration. The contribution of the neighboring streets is thus not taken into account and concentra-
tions of pollutants emitted in streets are expected to be lower than when there is a street network.

Table 1 and App. F present the influence of the neighboring streets for the three cases of the study. It is quantified using the
305 normalized mean error (NME) and bias (NMB) between the simulations without and with the neighboring streets. As expected,
without the street network, the concentrations are lower. The bias is between 12% and 21% for NO_2, 18% and 27% for NO_x
and 14% for BC. Biases are lower for OM and PM (2 %), because of stronger influence of background concentrations for those
compounds.

Table 1. Statistical indicators of the influence of the street network on concentrations simulated with MUNICH-hete for the street segment
of the Boulevard d'Alsace Lorraine with the monitoring station. Indicators are presented in Appendix B.

MUNICH-hete level			NO_2	NO_x	PM_{10}	$PM_{2.5}$	BC	OM
l1	With network	Mean concentration [$\mu g\,m^{-3}$]	58.92	104.74	24.58	22.18	1.84	6.13
	Without network	Mean concentration [$\mu g\,m^{-3}$]	51.50	85.46	24.15	21.97	1.58	5.98
		NME [%]	23.25	23.63	17.26	17.28	20.95	20.29
		NMB [%]	-12.58	-18.41	-1.75	-0.98	-14.02	-2.37
l2	With network	Mean concentration [$\mu g\,m^{-3}$]	47.81	75.36	21.94	20.08	1.42	5.30
	Without network	Mean concentration [$\mu g\,m^{-3}$]	42.67	62.34	21.77	20.04	1.25	5.25
		NME [%]	20.97	23.11	14.55	14.46	19.37	17.11
		NMB [%]	-10.74	-17.28	-0.75	-0.20	-12.15	-0.96
l3	With network	Mean concentration [$\mu g\,m^{-3}$]	37.97	52.63	19.91	18.41	1.09	4.69
	Without network	Mean concentration [$\mu g\,m^{-3}$]	35.65	47.01	19.89	18.44	1.02	4.69
		NME [%]	12.83	15.21	8.11	8.05	11.78	9.47
		NMB [%]	-6.10	-10.67	-0.08	0.15	-6.70	-0.12

6   Conclusions

310   The street-network model MUNICH v2.0 has been modified to introduce concentration heterogeneities in the street, and to better represent population exposure. To model the vertical gradients frequently observed, the streets were discretized with three levels, thus limiting the artificial dilution of emissions and concentrations. Based on a parameterization from OSPM, a ventilation zone is considered under specific conditions to represent horizontal heterogeneities. In order to test these developments, the heterogeneous version of MUNICH (MUNICH-hete) has been applied to two cases in Copenhagen, Denmark, with

315   comparisons to OSPM, and to one case near Paris, France. Overall, MUNICH-hete improves the comparison to observations compared to the homogeneous version. The errors to observations are reduced by up to 20 % for NO_x and 15 % for BC.

As expected, in MUNICH-hete, concentrations of compounds emitted by traffic (CO, NO_2, NO_x, PM_{10}, BC and OM) are higher at the bottom of the street than at the top. These increases can reach up to 60 % and 30 % for NO_2 and PM_{10} respectively. The intermediate level, serving as a buffer, presents concentrations higher or similar to the homogeneous version (MUNICH-

320   homo). Finally, concentrations in the highest level, in direct contact with the atmosphere above the street, are the lowest of the street. For the Danish cases, the low NO_2 concentrations observed in the lower levels could be related to the absence of volatile organic compounds in the model setup and the coarse vertical discretization limiting O_3 transport deep into the street.

A sensitivity study of the influence of the street network on concentrations in the streets shows the importance of considering neighboring streets in MUNICH. When no network is considered, concentrations in the street are lower due to the overestimated

325   impact of the atmosphere above. At the bottom of the street, concentrations of NO_2 and BC are reduced by up to 28 % and 14 % respectively without a network. PM and OM are less impacted with a reduction of about 2 % due to a strong influence of non-traffic sources.

For the next step, the ventilation zone will be fully discretized vertically to facilitate the penetration of background concentrations to the bottom of the street. The horizontal exchange fluxes between the two zones will be also be modelled. Deposition

330   and resuspension processes that were not considered in this development will be added. Finally, the fluxes that are currently assumed to be vertically homogeneous will be discretized.

Code and data availability. MUNICH-hete is available at Sarica et al. (2023). The configuration files, the input data and also the scripts to generate the figures and statistics are available at Sarica et al. (2023).

Appendix A: Volumes of the recirculation and ventilation zones

335 The algorithm used in the heterogeneous version of MUNICH to compute the volumes of the recirculation and ventilation zones is based on the parameterization of OSPM (Berkowicz et al., 1997; Berkowicz, 2000a; Ottosen et al., 2015). This algorithm is applied at the beginning of each time step as the size of the recirculation zone is dependent on wind speed and direction. Fig A1 presents the shape of the recirculation zone and the associated parameters.
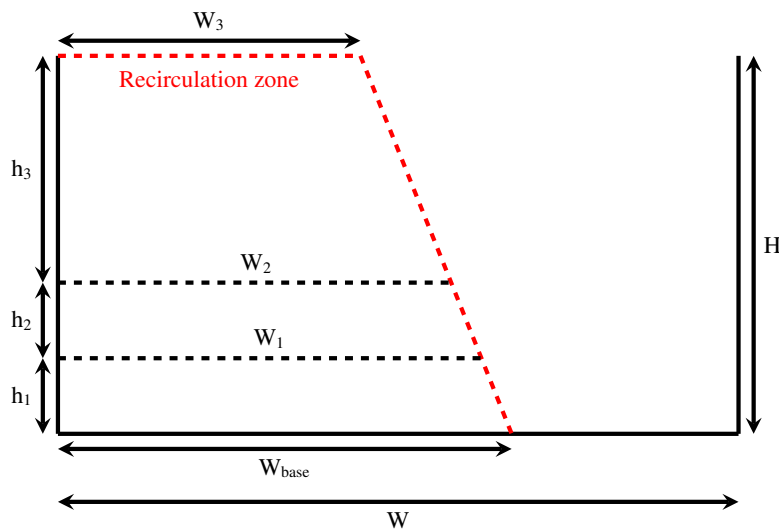

Figure A1. Representation of the recirculation zone in the heterogeneous version of MUNICH.

The first step is to compute the length of the vortex in the direction of the wind:

$$L_{\text{vortex}} = 2Hf \tag{A1}$$

with H the height of the street and

$$f = \begin{cases} 1 \ if \ u_{\text{roof}} \ \geq \ 2ms^{-1} \\ \sqrt{0.5u_{\text{roof}}} \ if \ u_{\text{roof}} \ < \ 2ms^{-1} \end{cases} \tag{A2}$$

with u_{roof} the wind speed at roof level.

The width of the trapeze base is the projection of L_{vortex} in the street:

$$W_{base} = L_{\text{vortex}} sin(\theta)) \tag{A3}$$

with θ the angle between the wind direction and the street orientation.

The width of the trapeze top is equal to half of the base:

$$W_3 = \frac{L_{\text{vortex}} sin(\theta)}{2} \tag{A4}$$

Knowing these lengths and using algebraic considerations, the widths W_1 and W_2 can be calculated:

$$\begin{cases} W_1 = W_3 + \dfrac{(h_2 + h_3)\Delta W}{H} \\ W_2 = W_3 + \dfrac{h_3 \Delta W}{H} \end{cases} \tag{A5}$$

with $\Delta W = W_{base} - W_3$

The horizontal surfaces for vertical exchanges between the levels and with the concentrations above the street are calculated as followed:

$$\begin{cases} S_1^h = W_1 L \\ S_2^h = W_2 L \\ S_3^h = W_3 L \end{cases} \tag{A6}$$

with L the street length.

The vertical surfaces for advection via intersections are determined with:

$$\begin{cases} S_1^v = \dfrac{W_1 (h_1)^2 (W_{base} - W_1)}{2} \\ S_2^v = \dfrac{W_2 (h_2)^2 (W_1 - W_2)}{2} \\ S_3^v = \dfrac{W_3 (h_3)^2 (W_2 - W_3)}{2} \end{cases} \tag{A7}$$

Finally, the volumes associated to each level of the recirculation zone are :

$$\begin{cases} V_1 = h_1 L \left(W_1 + \dfrac{(W_{base} - W_1)}{2} \right) \\ V_2 = h_2 L \left(W_2 + \dfrac{(W_1 - W_2)}{2} \right) \\ V_3 = h_3 L \left(W_3 + \dfrac{(W_2 - W_3)}{2} \right) \end{cases} \tag{A8}$$

In the current version of MUNICH-hete, it is assumed that traffic emissions are all affected to the recirculation zone. Therefore, its base W_{base} has to be superior or equal to the street width W. If it is not the case, the recirculation zone is considered to fill the whole street volume.

When considered, the other widths are also limited by the street width:

$$\begin{cases} W_1 = min(W, W_1) \\ W_2 = min(W, W_2) \\ W_3 = min(W, W_3) \end{cases} \tag{A9}$$

Appendix B: Statistical indicators

For evaluation of the simulations to observations, the following statistical indicators are used. o and s represent the observed and the simulated concentrations respectively. The overbar represents the average.

– Mean fractional error (MFE):

$$MFE = 2 \times \overline{\left(\frac{|s-o|}{s+o} \right)}$$

– Mean fractional bias (MFB):

$$MFB = 2 \times \overline{\left(\frac{s-o}{s+o} \right)}$$

– Factor of 2 (FAC2): fraction of data that satisfy $0.5 \leq \frac{s}{o} \leq 2.0$

For comparison of the simulations, the normalized mean bias (NMB) and normalized mean error (NME) are used. X represents concentrations with X_0 the reference simulation and X_i the compared simulation. The overbar represents the average.

– Normalized mean bias:

$$NMB = \frac{\overline{(X_i - X_0)}}{\overline{X_0}}$$

– Normalized mean error:

$$NME = \frac{\overline{|X_i - X_0|}}{\overline{X_0}}$$

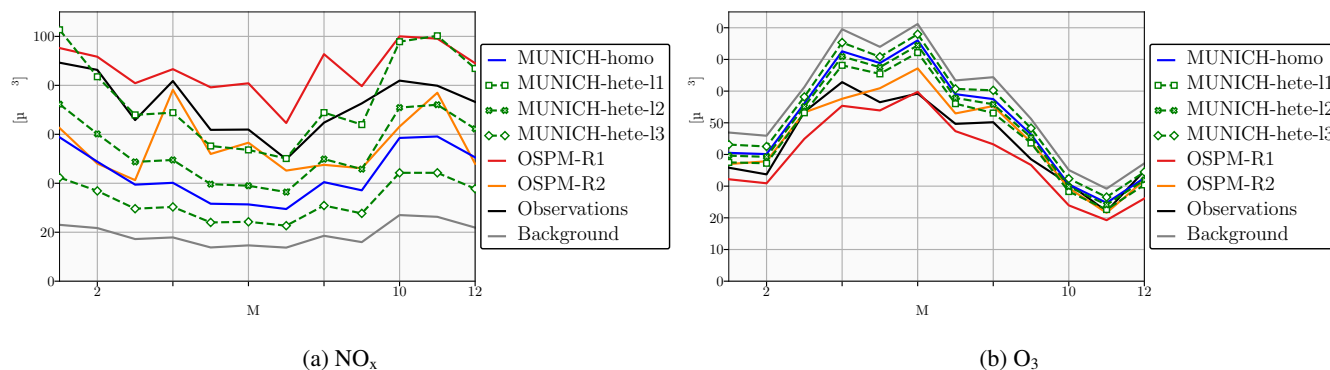## Appendix C: Additional information for HCAB

(a) NO$_x$

(b) O$_3$

Figure C1. Monthly-average concentrations (in µg m^{-3}) of NO$_x$ (a) and O$_3$ (b) at HCAB monitoring station. The solid blue line represents the homogeneous version of MUNICH. The three green dashed lines represents the three levels of the heterogeneous version of MUNICH, the lowest level (l1) with square markers, the intermediate level (l2) with cross markers and the top level (l3) with diamond markers. The solid red line represents the OSPM receptor that is close to the measurement station and the solid orange line the second OSPM receptor located on the other side of the street. The observations are in solid black and the background concentrations in solid grey

Table C1. Statistical indicators of the evaluation of the hourly simulated concentrations to observations at HCAB monitoring station. Indicators are presented in Appendix B.

		CO	NO_2	NO_x	O_3
Observations	Mean concentration [$\mu g\,m^{-3}$]	285.35	34.64	72.30	44.33
MUNICH-homo	Mean concentration [$\mu g\,m^{-3}$]	210.88	25.34	43.77	50.44
	MFE	0.36	0.48	0.55	0.38
	MFB	-0.29	-0.29	-0.42	0.14
	FAC2	0.91	0.73	0.63	0.83
MUNICH-hete-l1	Mean concentration [$\mu g\,m^{-3}$]	249.29	32.37	74.95	47.34
	MFE	0.28	0.35	0.35	0.37
	MFB	-0.14	-0.06	0.05	0.07
	FAC2	0.96	0.87	0.86	0.84
MUNICH-hete-l2	Mean concentration [$\mu g\,m^{-3}$]	223.39	27.69	53.86	49.36
	MFE	0.32	0.42	0.43	0.37
	MFB	-0.24	-0.21	-0.24	0.12
	FAC2	0.93	0.80	0.78	0.83
MUNICH-hete-l3	Mean concentration [$\mu g\,m^{-3}$]	197.59	21.87	32.90	52.59
	MFE	0.39	0.57	0.73	0.39
	MFB	-0.34	-0.43	-0.65	0.20
	FAC2	0.88	0.61	0.42	0.82
OSPM-R1	Mean concentration [$\mu g\,m^{-3}$]	272.86	40.59	86.60	39.50
	MFE	0.26	0.34	0.40	0.35
	MFB	-0.05	0.19	0.21	-0.11
	FAC2	0.96	0.87	0.82	0.86
OSPM-R2	Mean concentration [$\mu g\,m^{-3}$]	227.84	30.53	55.43	45.77
	MFE	0.33	0.46	0.61	0.36
	MFB	-0.23	-0.16	-0.33	0.05
	FAC2	0.93	0.74	0.61	0.84

Geoscientific
Model Development
Discussions

EGU

380 **Appendix D: Additional information for JGTV**

(a) NO$_x$

(b) O$_3$

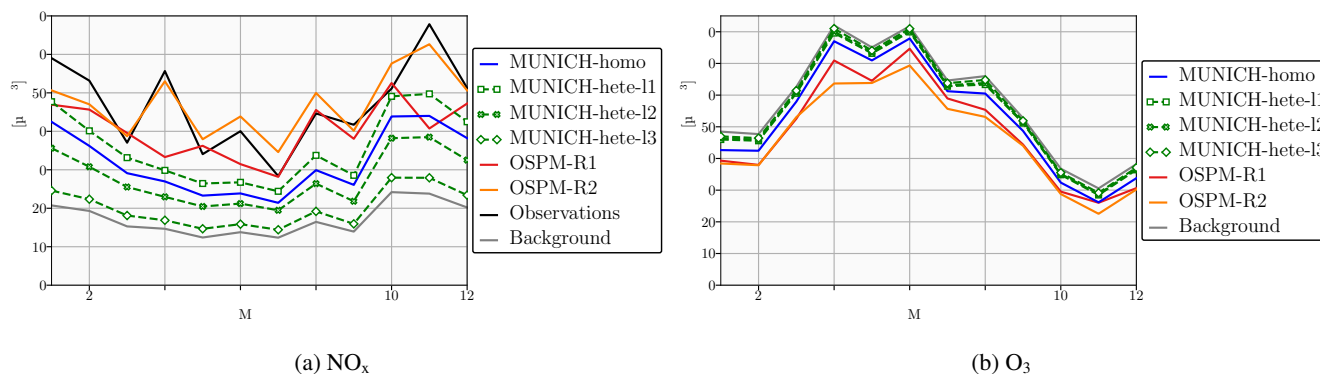**Figure D1.** Monthly-average concentrations (in µg m^{-3}) of NO$_x$ (a) and O$_3$ (b) at JGTV monitoring station. The solid blue line represents the homogeneous version of MUNICH. The three green dashed lines represents the three levels of the heterogeneous version of MUNICH, the lowest level (l1) with square markers, the intermediate level (l2) with cross markers and the top level (l3) with diamond markers. The solid orange line represents the OSPM receptor that is close to the measurement station and the solid red line the second OSPM receptor located on the other side of the street. The observations are in solid black and the background concentrations in solid grey

Table D1. Statistical indicators of the evaluation of the hourly simulated concentrations to observations at JGTV monitoring station. Indicators are presented in Appendix B.

		NO_2	NO_x
Observations	Mean concentration [µg m^{-3}]	24.50	46.94
MUNICH-homo	Mean concentration [µg m^{-3}]	21.69	32.10
	MFE	0.46	0.53
	MFB	-0.03	-0.19
	FAC2	0.75	0.66
MUNICH-hete-l1	Mean concentration [µg m^{-3}]	19.77	35.99
	MFE	0.49	0.51
	MFB	-0.13	-0.11
	FAC2	0.75	0.68
MUNICH-hete-l2	Mean concentration [µg m^{-3}]	18.37	27.78
	MFE	0.52	0.58
	MFB	-0.20	-0.32
	FAC2	0.71	0.61
MUNICH-hete-l3	Mean concentration [µg m^{-3}]	16.81	20.10
	MFE	0.57	0.74
	MFB	-0.29	-0.58
	FAC2	0.68	0.46
OSPM-R1	Mean concentration [µg m^{-3}]	25.60	40.46
	MFE	0.53	0.63
	MFB	0.15	0.03
	FAC2	0.67	0.56
OSPM-R2	Mean concentration [µg m^{-3}]	28.41	47.21
	MFE	0.41	0.42
	MFB	0.25	0.18
	FAC2	0.80	0.79

Appendix E: Additional information for the district of Le Perreux-sur-Marne
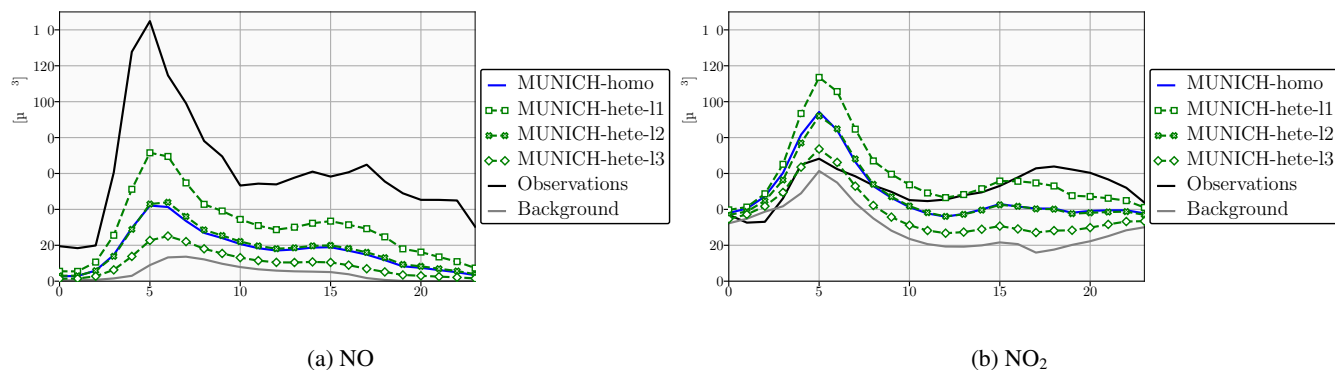

(a) NO

(b) NO$_2$

Figure E1. Average daily profile of the concentrations of NO (a) and NO$_2$ (b) over the simulation period at the Boulevard d'Alsace Lorraine monitoring station. The solid blue line represents the homogeneous version of MUNICH. The three green dashed lines represents the three levels of the heterogeneous version of MUNICH, the lowest level (l1) with square markers, the intermediate level (l2) with cross markers and the top level (l3) with diamond markers. The observations are in solid black and the background concentrations in solid grey

Table E1. Statistical indicators of the evaluation of the hourly simulated concentrations to observations at the Boulevard d'Alsace Lorraine monitoring station. Indicators are presented in Appendix B.

		NO_2	NO_x	PM_{10}	$PM_{2.5}$	BC
Observations	Mean concentration [µg m^{-3}]	52.16	147.19	23.42	12.72	6.10
MUNICH-homo	Mean concentration [µg m^{-3}]	48.49	74.62	21.89	20.06	1.41
	MFE	0.36	0.65	0.38	0.53	1.17
	MFB	-0.11	-0.60	-0.08	0.38	-1.16
	FAC2	0.87	0.52	0.84	0.67	0.09
MUNICH-hete-l1	Mean concentration [µg m^{-3}]	58.92	104.74	24.58	22.18	1.84
	MFE	0.33	0.41	0.37	0.57	1.01
	MFB	0.08	-0.30	0.03	0.47	-1.00
	FAC2	0.91	0.80	0.86	0.61	0.16
MUNICH-hete-l2	Mean concentration [µg m^{-3}]	47.81	75.36	21.94	20.08	1.42
	MFE	0.36	0.64	0.38	0.53	1.17
	MFB	-0.12	-0.59	-0.08	0.38	-1.16
	FAC2	0.86	0.53	0.84	0.67	0.08
MUNICH-hete-l3	Mean concentration [µg m^{-3}]	37.97	52.63	19.91	18.41	1.09
	MFE	0.49	0.90	0.42	0.50	1.30
	MFB	-0.35	-0.88	-0.18	0.30	-1.30
	FAC2	0.71	0.25	0.80	0.70	0.06

(a) MUNICH-homo, NO$_2$ concentration

(b) Relative differences of NO$_2$ between
MUNICH-hete-l1 and MUNICH-homo

(c) MUNICH-homo, PM$_{10}$ concentration

(d) Relative differences of PM$_{10}$ between
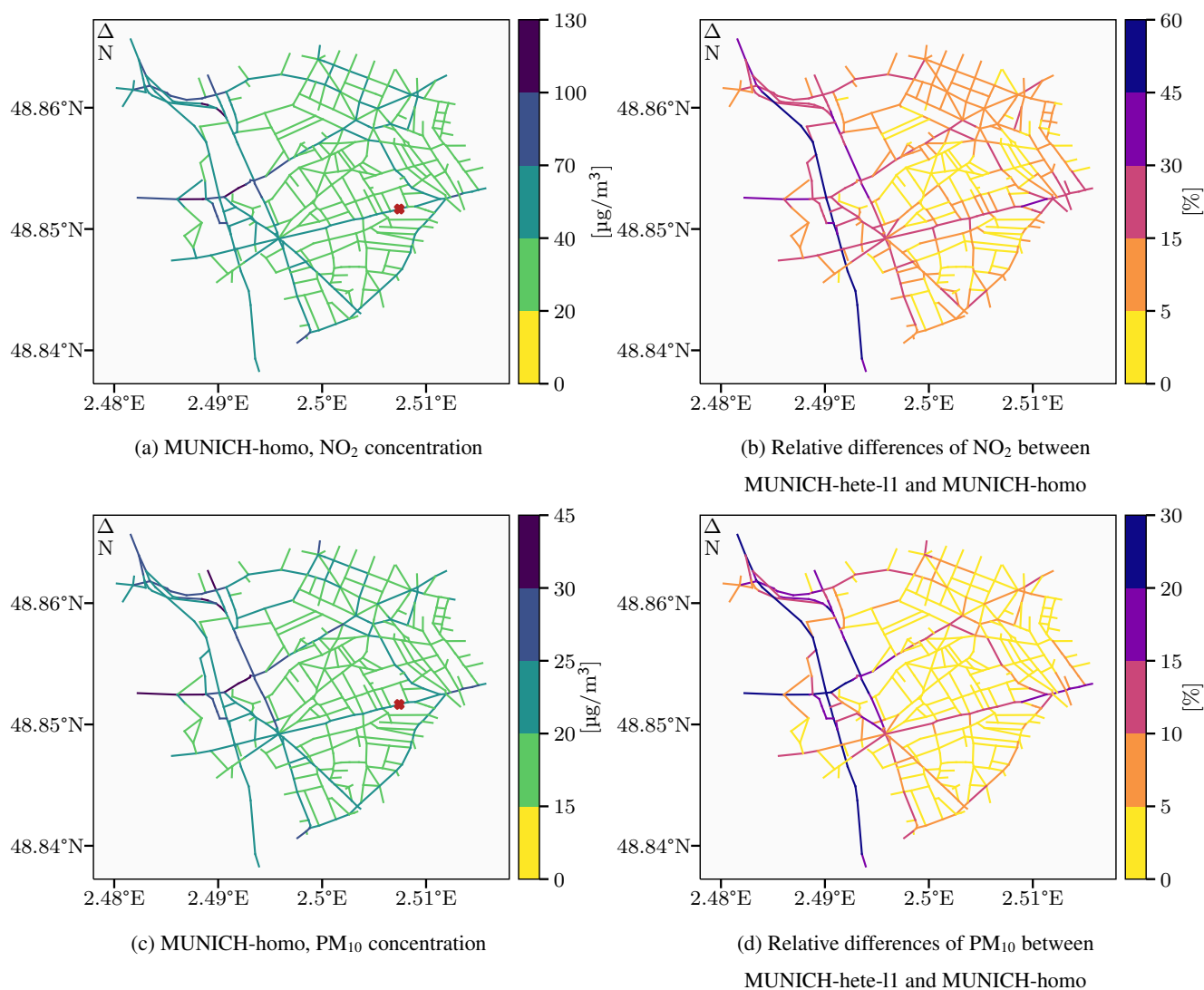MUNICH-hete-l1 and MUNICH-homo

Figure E2. NO$_2$ and PM$_{10}$ time-averaged concentrations (in µg m^{-3}) for MUNICH-homo in the left panel for the district of Le Perreux-sur-Marne. Relative differences (in %) between the first level of MUNICH-hete and MUNICH-homo for PM$_{10}$ in the right panel for the district of Le Perreux-sur-Marne. A positive relative difference indicates higher concentrations for MUNICH-hete. The brown cross on panels (a) and (c) represents the position of the measurement station.

Appendix F: Additional information for the sensitivity analysis

Table F1. Statistical indicators of the influence of the street network on concentrations simulated with MUNICH-hete for the street segment HCAB with the monitoring station. Indicators are presented in Appendix B.

MUNICH-hete level			CO	NO$_2$	NO$_x$	O$_3$
l1	With network	Mean concentration [µg m^{-3}]	249.29	32.37	74.95	47.34
	Without network	Mean concentration [µg m^{-3}]	214.27	23.28	46.69	52.98
		NME [%]	14.05	28.06	37.70	11.90
		NMB [%]	-14.05	-28.06	-37.70	11.90
l2	With network	Mean concentration [µg m^{-3}]	223.39	27.69	53.86	49.36
	Without network	Mean concentration [µg m^{-3}]	198.12	20.78	33.47	53.79
		NME [%]	11.32	24.95	37.86	8.99
		NMB [%]	-11.32	-24.95	-37.86	8.99
l3	With network	Mean concentration [µg m^{-3}]	197.59	21.87	32.90	52.59
	Without network	Mean concentration [µg m^{-3}]	186.96	18.65	24.33	54.78
		NME [%]	5.38	14.73	26.05	4.17
		NMB [%]	-5.38	-14.73	-26.05	4.17

Table F2. Statistical indicators of the influence of the street network on concentrations simulated with MUNICH-hete for the street segment JGTV with the monitoring station. Indicators are presented in Appendix B.

MUNICH-hete level			CO	NO$_2$	NO$_x$	O$_3$
l1	With network	Mean concentration [µg m^{-3}]	201.21	19.77	35.99	55.19
	Without network	Mean concentration [µg m^{-3}]	189.24	17.46	27.56	56.45
		NME [%]	6.09	12.38	23.63	3.13
		NMB [%]	-5.95	-11.70	-23.43	2.29
l2	With network	Mean concentration [µg m^{-3}]	189.49	18.37	27.78	55.54
	Without network	Mean concentration [µg m^{-3}]	181.01	16.52	21.80	56.64
		NME [%]	4.71	10.87	21.85	2.85
		NMB [%]	-4.47	-10.03	-21.53	1.99
l3	With network	Mean concentration [µg m^{-3}]	178.59	16.81	20.10	56.12
	Without network	Mean concentration [µg m^{-3}]	176.03	15.92	18.30	56.80
		NME [%]	1.84	6.16	9.57	1.83
		NMB [%]	-1.43	-5.30	-8.92	1.21

385

References

Amato, F., Pérez, N., López, M., Ripoll, A., Alastuey, A., Pandolfi, M., Karanasiou, A., Salmatonidis, A., Padoan, E., Frasca, D., Marcoccia, M., Viana, M., Moreno, T., Reche, C., Martins, V., Brines, M., Minguillón, M., Ealo, M., Rivas, I., van Drooge, B., Benavides, J., Craviotto, J., and Querol, X.: Vertical and horizontal fall-off of black carbon and NO2 within urban blocks, Sci. Total Environ., 686, 236–245, https://doi.org/10.1016/j.scitotenv.2019.05.434, 2019.

Archambeau, F., Méchitoua, N., and Sakiz, M.: Code Saturne: A Finite Volume Code for the computation of turbulent incompressible flows - Industrial Applications, International Journal on Finite Volumes, 1, http://www.latp.univ–mrs.fr/IJFV/spip.php?article3, https://hal.science/hal-01115371, 2004.

Atkinson, R.: Atmospheric chemistry of VOCs and NOx, Atmos. Environ., 34, 2063–2101, https://doi.org/10.1016/S1352-2310(99)00460-4, 2000.

Berkowicz, R.: OSPM - a parameterised street pollution model, Environ. Monit. Assess., 65, 323–331, https://doi.org/10.1023/A:1006448321977, 2000a.

Berkowicz, R.: A simple model for urban background pollution, Environ. Monit. Assess., 65, 259–267, https://doi.org/10.1023/a:1006466025186, 2000b.

Berkowicz, R., Hertel, O., Larsen, S., Sørensen, N., and Nielsen, M.: Modelling traffic pollution in streets, , https://backend.orbit.dtu.dk/ws/portalfiles/portal/128001317/Modelling_traffic_pollution_in_streets.pdf, (last visited 2023-02-13), 1997.

Cimorelli, A., Perry, S., Venkatram, A., Weil, J., Paine, R., Wilson, R., Lee, R., Peters, W., Brode, R., and Paumier, J.: AERMOD: description of model formulation, US Environmental Protection Agency, Tech. rep., EPA-454/R-03-004, 2004.

Coceal, O. and Belcher, S.: A canopy model of mean winds through urban areas, Q.J.R. Meteorol. Soc., 130, 1349–1372, https://doi.org/10.1256/qj.03.40, 2004.

Collett, R. S. and Oduyemi, K.: Air quality modelling: a technical review of mathematical approaches, Meteorol. Appl., 4, 235–246, https://doi.org/10.1017/S1350482797000455, 1997.

Conti, G. O., Heibati, B., Kloog, I., Fiore, M., and Ferrante, M.: A review of AirQ Models and their applications for forecasting the air pollution health outcomes, Environ. Sci. Pollut. Res., 24, 6426–6445, https://doi.org/10.1007/s11356-016-8180-1, 2017.

Dai, Y., Cai, X., Zhong, J., and MacKenzie, A. R.: Modelling chemistry and transport in urban street canyons: Comparing offline multi-box models with large-eddy simulation, Atmospheric Environment, 264, 118 709, https://doi.org/10.1016/j.atmosenv.2021.118709, 2021.

de la Paz, D., Borge, R., Vedrenne, M., Lumbreras, J., Amato, F., Karanasiou, A., Boldo, E., and Moreno, T.: Implementation of road dust resuspension in air quality simulations of particulate matter in Madrid (Spain), Front. Environ. Sci., 3, https://doi.org/10.3389/fenvs.2015.00072, 2015.

El-Harbawi, M.: Air quality modelling, simulation, and computational methods: a review, Environ. Rev., 21, 149–179, https://doi.org/10.1139/er-2012-0056, 2013.

Falasca, S. and Curci, G.: High-resolution air quality modeling: Sensitivity tests to horizontal resolution and urban canopy with WRF-CHIMERE, Atmos. Environ., 187, 241–254, https://doi.org/10.1016/j.atmosenv.2018.05.048, 2018.

Fuller, R., Landrigan, P. J., Balakrishnan, K., Bathan, G., Bose-O'Reilly, S., Brauer, M., Caravanos, J., Chiles, T., Cohen, A., Corra, L., Cropper, M., Ferraro, G., Hanna, J., Hanrahan, D., Hu, H., Hunter, D., Janata, G., Kupka, R., Lanphear, B., Lichtveld, M., Martin, K., Mustapha, A., Sanchez-Triana, E., Sandilya, K., Schaefli, L., Shaw, J., Seddon, J., Suk, W., Téllez-Rojo, M. M., and Yan, C.: Pollution and health: a progress update, Lancet Planet. Health, 6, e535–e547, https://doi.org/10.1016/S2542-5196(22)00090-0, 2022.

Gao, Z., Bresson, R., Qu, Y., Milliez, M., de Munck, C., and Carissimo, B.: High resolution unsteady RANS simulation of wind, ther-
mal effects and pollution dispersion for studying urban renewal scenarios in a neighborhood of Toulouse, Urban Clim., 23, 114–130,
https://doi.org/10.1016/j.uclim.2016.11.002, iCUC9: The 9th International Conference on Urban Climate, 2018.

Hood, C., Stocker, J., Seaton, M., Johnson, K., O'Neill, J., Thorne, L., and Carruthers, D.: Comprehensive evaluation of an advanced street
canyon air pollution model, J. Air Waste Manag. Assoc., 71, 247–267, https://doi.org/10.1080/10962247.2020.1803158, 2021.

Khan, S. and Quamrul, H.: Review of developments in air quality modelling and air quality dispersion models, J. Environ. Eng. Sci., 16,
1–10, https://doi.org/10.1680/jenes.20.00004, 2021.

Kim, Y., Wu, Y., Seigneur, C., and Roustan, Y.: Multi-scale modeling of urban air pollution: development and application of a Street-in-Grid
model (v1.0) by coupling MUNICH (v1.0) and Polair3D (v1.8.1), Geosci. Mod. Dev., 11, 611–629, https://doi.org/10.5194/gmd-11-611-
2018, 2018.

Kim, Y., Lugon, L., Maison, A., Sarica, T., Roustan, Y., Valari, M., Zhang, Y., André, M., and Sartelet, K.: MUNICH v2.0: a street-network
model coupled with SSH-aerosol (v1.2) for multi-pollutant modelling, Geosci. Mod. Dev., 15, 7371–7396, https://doi.org/10.5194/gmd-
15-7371-2022, 2022.

Kwak, K.-H. and Baik, J.-J.: A CFD modeling study of the impacts of NOx and VOC emissions on reactive pollutant dispersion in and above
a street canyon, Atmos. Environ., 46, 71–80, https://doi.org/https://doi.org/10.1016/j.atmosenv.2011.10.024, 2012.

Landrigan, P. J., Fuller, R., Acosta, N. J. R., Adeyi, O., Arnold, R., Basu, N. N., Baldé, A. B., Bertollini, R., Bose-O'Reilly, S., Boufford,
J. I., Breysse, P. N., Chiles, T., Mahidol, C., Coll-Seck, A. M., Cropper, M. L., Fobil, J., Fuster, V., Greenstone, M., Haines, A., Hanrahan,
D., Hunter, D., Khare, M., Krupnick, A., Lanphear, B., Lohani, B., Martin, K., Mathiasen, K. V., McTeer, M. A., Murray, C. J. L.,
Ndahimananjara, J. D., Perera, F., Potočnik, J., Preker, A. S., Ramesh, J., Rockström, J., Salinas, C., Samson, L. D., Sandilya, K., Sly,
P. D., Smith, K. R., Steiner, A., Stewart, R. B., Suk, W. A., van Schayck, O. C. P., Yadama, G. N., Yumkella, K., and Zhong, M.: The
Lancet Commission on pollution and health, Lancet, 391, 462–512, https://doi.org/10.1016/S0140-6736(17)32345-0, 2018.

Lateb, M., Meroney, R., Yataghene, M., Fellouah, H., Saleh, F., and Boufadel, M.: On the use of numerical modelling for near-field pollutant
dispersion in urban environments - A review, Environ. Pollut., 208, 271–283, https://doi.org/https://doi.org/10.1016/j.envpol.2015.07.039,
special Issue: Urban Health and Wellbeing, 2016.

Leighton, P. A.: Photochemistry of air pollution, Academic Press, New York, 1961.

Liang, M., Chao, Y., Tu, Y., and Xu, T.: Vehicle Pollutant Dispersion in the Urban Atmospheric Environment: A Review of Mechanism,
Modeling, and Application, Atmosphere, 14, https://doi.org/10.3390/atmos14020279, 2023.

Lin, C., Wang, Y., Ooka, R., Flageul, C., Kim, Y., Kikumoto, H., Wang, Z., and Sartelet, K.: Modelling of street-scale pollutant
dispersion by coupled simulation of chemical reaction, aerosol dynamics, and CFD, Atmos. Chem. Phys. Discuss., 2022, 1–32,
https://doi.org/10.5194/acp-2022-365, 2022.

Lugon, L., Sartelet, K., Kim, Y., Vigneron, J., and Chrétien, O.: Nonstationary modeling of NO2, NO and NOX in Paris using the
Street-in-Grid model: coupling local and regional scales with a two-way dynamic approach, Atmos. Chem. Phys., 20, 7717–7740,
https://doi.org/10.5194/acp-20-7717-2020, 2020.

Lugon, L., Sartelet, K., Kim, Y., Vigneron, J., and Chrétien, O.: Simulation of primary and secondary particles in the streets of Paris using
MUNICH, Faraday Discuss., 226, 432–456, https://doi.org/10.1039/D0FD00092B, 2021a.

Lugon, L., Vigneron, J., Debert, C., Chrétien, O., and Sartelet, K.: Black carbon modeling in urban areas: investigating the influence of
resuspension and non-exhaust emissions in streets using the Street-in-Grid model for inert particles (SinG-inert), Geosci. Mod. Dev., 14,
7001–7019, https://doi.org/10.5194/gmd-14-7001-2021, 2021b.

Maison, A., Flageul, C., Carissimo, B., Tuzet, A., and Sartelet, K.: Parametrization of Horizontal and Vertical Transfers for the Street-Network Model MUNICH Using the CFD Model Code_Saturne, Atmosphere, 13, 527, https://doi.org/10.3390/atmos13040527, 2022.

465 Mallet, V., Quélo, D., Sportisse, B., Ahmed de Biasi, M., Debry, E., Korsakissok, I., Wu, L., Roustan, Y., Sartelet, K., Tombette, M., and Foudhil, H.: Technical Note: The air quality modeling system Polyphemus, Atmos. Chem. Phys., 7, 5479–5487, https://doi.org/10.5194/acp-7-5479-2007, 2007.

McHugh, C., Carruthers, D., and Edmunds, H.: ADMS and ADMS–Urban, Int J Environ Pollut, 8, 438–440, https://doi.org/10.1504/IJEP.1997.028193, 1997.

470 Menut, L., Bessagnet, B., Briant, R., Cholakian, A., Couvidat, F., Mailler, S., Pennel, R., Siour, G., Tuccella, P., Turquety, S., and Valari, M.: The CHIMERE v2020r1 online chemistry-transport model, Geosci. Mod. Dev., 14, 6781–6811, https://doi.org/10.5194/gmd-14-6781-2021, 2021.

Olesen, H., Ketzel, M., Jensen, S., Løfstrøm, P., Im, U., and Becker, T.: User Guide to OML-Highway. A tool for air pollution assessments along highways., Tech. rep., Aarhus University, DCE – Danish Centre for Environment and Energy, https://dce2.au.dk/pub/TR59.pdf, (last 475 visited 2023-02-14), 2015.

Ottosen, T.-B., Kakosimos, K. E., Johansson, C., Hertel, O., Brandt, J., Skov, H., Berkowicz, R., Ellermann, T., Jensen, S. S., and Ketzel, M.: Analysis of the impact of inhomogeneous emissions in the Operational Street Pollution Model (OSPM), Geosci. Mod. Dev., 8, 3231–3245, https://doi.org/10.5194/gmd-8-3231-2015, 2015.

Rood, A. S.: Performance evaluation of AERMOD, CALPUFF, and legacy air dispersion models using the Winter Validation Tracer Study 480 dataset, Atmos. Environ., 89, 707–720, https://doi.org/10.1016/j.atmosenv.2014.02.054, 2014.

Sanchez, B., Santiago, J.-L., Martilli, A., Palacios, M., and Kirchner, F.: CFD modeling of reactive pollutant dispersion in simplified urban configurations with different chemical mechanisms, Atmos. Chem. Phys., 16, 12 143–12 157, https://doi.org/10.5194/acp-16-12143-2016, 2016.

Sarica, T., Sartelet, K., Roustan, Y., Kim, Y., Lugon, L., André, M., Marques, B., D'Anna, B., Chaillou, C., and Larrieu, C.: Modelling Pollu-485 tant Concentrations in Streets: A Sensitivity Analysis to Asphalt and Traffic Related Emissions, in: Air Pollution Modeling and its Application XXVIII, edited by Mensink, C. and Jorba, O., pp. 287–293, Springer International Publishing, Cham, https://doi.org/10.1007/978-3-031-12786-1_39, 2022.

Sarica, T., Maison, A., Roustan, Y., Ketzel, M., Jensen, S. S., Kim, Y., and Sartelet, K.: The Model of Urban Network of Intersecting Canyons and Highways (MUNICH), Zenodo, https://doi.org/10.5281/zenodo.7778271, 2023.

490 Sartelet, K., Zhu, S., Moukhtar, S., André, M., André, J., Gros, V., Favez, O., Brasseur, A., and Redaelli, M.: Emission of intermediate, semi and low volatile organic compounds from traffic and their impact on secondary organic aerosol concentrations over Greater Paris, Atmos. Environ., 180, 126–137, https://doi.org/10.1016/j.atmosenv.2018.02.031, 2018.

Sartelet, K., Couvidat, F., Wang, Z., Flageul, C., and Kim, Y.: SSH-Aerosol v1.1: A Modular Box Model to Simulate the Evolution of Primary and Secondary Aerosols, Atmosphere, 11, https://doi.org/10.3390/atmos11050525, 2020.

495 Skamarock, W., Klemp, J., Dudhia, J., Gill, D., Barker, D., Wang, W., Huang, X.-Y., and Duda, M.: A Description of the Advanced Research WRF Version 3, Tech. rep., UCAR/NCAR, https://doi.org/10.5065/D68S4MVH, 2008.

Solazzo, E., Cai, X., and Vardoulakis, S.: Modelling wind flow and vehicle-induced turbulence in urban streets, Atmos. Environ., 42, 4918–4931, https://doi.org/https://doi.org/10.1016/j.atmosenv.2008.02.032, 2008.

Soulhac, L., Garbero, V., Salizzoni, P., Mejean, P., and Perkins, R.: Flow and dispersion in street intersections, Atmos. Environ., 43, 2981–500 2996, https://doi.org/10.1016/j.atmosenv.2009.02.061, 2009.

Soulhac, L., Salizzoni, P., Cierco, F.-X., and Perkins, R.: The model SIRANE for atmospheric urban pollutant dispersion; part I, presentation of the model, Atmos. Environ., 45, 7379–7395, https://doi.org/10.1016/j.atmosenv.2011.07.008, 2011.

Soulhac, L., Fellini, S., Nguyen, C. V., and Salizzoni, P.: Evaluation of Photostationary and Non-Photostationary Operational Models for NOX Pollution in a Street Canyon, Atmos. Environ., 297, 119 589, https://doi.org/10.1016/j.atmosenv.2023.119589, 2023.

505 United Nations: World Urbanization Prospects: The 2018 Revision (ST/ESA/SER.A/420), Tech. rep., United Nations, https://population.un.org/wup/Publications/Files/WUP2018-Report.pdf, 2019.

Vardoulakis, S., Fisher, B., Pericleous, K., and Gonzalez-Flesca, N.: Modelling air quality in street canyons: a review, Atmos. Environ., 37, 155–182, https://doi.org/10.1016/S1352-2310(02)00857-9, 2003.

Vardoulakis, S., Solazzo, E., and Lumbreras, J.: Intra-urban and street scale variability of BTEX, NO2 and O3 in Birmingham, UK: Implica-
510 tions for exposure assessment, Atmos. Environ., 45, 5069–5078, https://doi.org/10.1016/j.atmosenv.2011.06.038, 2011.

Wang, W.: Analytically modelling mean wind and stress profiles in canopies, Bound.-Lay. Meteorol., 151, 239–256, https://doi.org/10.1007/s10546-013-9899-6, 2014.

Wolf, T., Pettersson, L. H., and Esau, I.: A very high-resolution assessment and modelling of urban air quality, Atmos. Chem. Phys., 20, 625–647, https://doi.org/10.5194/acp-20-625-2020, 2020.

515 Wong, D., Pleim, J., Mathur, R., Binkowski, F., Otte, T., Gilliam, R., Pouliot, G., Xiu, A., and Kang, D.: WRF-CMAQ two-way coupled system with aerosol feedback: software development and preliminary results., Geosci. Mod. Dev., 5, 299–312, https://doi.org/10.5194/gmd-5-299-2012, 2012.

Xie, S., Zhang, Y., Qi, L., and Tang, X.: Spatial distribution of traffic-related pollutant concentrations in street canyons, Atmos. Environ., 37, 3213–3224, https://doi.org/10.1016/S1352-2310(03)00321-2, 2003.

520 Zhong, J., Cai, X.-M., and Bloss, W. J.: Large eddy simulation of reactive pollutants in a deep urban street canyon: Coupling dynamics with O3-NOx-VOC chemistry, Environmental Pollution, 224, 171–184, https://doi.org/https://doi.org/10.1016/j.envpol.2017.01.076, 2017.